PLANETARY SCIENCE

Low-temperature synthesis of polycyclic aromatic hydrocarbons in Titan's surface ices and on airless bodies

Matthew J. Abplanalp[1,2], Robert Frigge[1,2], Ralf I. Kaiser[1,2]*

Titan's equatorial dunes represent the most monumental surface structures in our Solar System, but the chemical composition of their dark organics remains a fundamental, unsolved enigma, with solid acetylene detected near the dunes implicated as a key feedstock. Here, we reveal in laboratory simulation experiments that aromatics such as benzene, naphthalene, and phenanthrene—prospective building blocks of the organic dune material—can be efficiently synthesized via galactic cosmic ray exposure of low-temperature acetylene ices on Titan's surface, hence challenging conventional wisdom that aromatic hydrocarbons are formed solely in Titan's atmosphere. These processes are also of critical importance in unraveling the origin and chemical composition of the dark surfaces of airless bodies in the outer Solar System, where hydrocarbon precipitation from the atmosphere cannot occur. This finding notably advances our understanding of the distribution of carbon throughout our Solar System such as on Kuiper belt objects like Makemake.

INTRODUCTION

For the past two decades, the Cassini-Huygens mission to Saturn's moon Titan—the only Solar System body besides Earth with a solid surface, surface liquids, and a thick atmosphere with a pressure of about 1.45 atm at surface level (*1*)—has transformed our understanding of the origin and evolution of the Solar System (*2*). This mission exposed Titan as a world with remarkable Earth-like features encompassing vast hydrocarbon lakes and seas dominated by methane (CH_4) and ethane (C_2H_6) (*2*), along with lava-like landscapes intermixed with craters and mountains (*3*). Titan's active atmosphere (*1*, *4*) and dynamical weather system (*5*) together with hydrocarbon rain cycles (*2*) further illuminate the similarities between Titan and Earth (*4*). Titan's most eminent surface topographies are vast longitudinal dunes across the equatorial deserts between 30°N and 30°S, reaching heights of nearly 100 m in Shangri-La Sand Sea (*6*). However, whereas Earth's extant dunes are made of silicates, optical and near-infrared images from the Cassini's Visual and Infrared Mapping Spectrometer (VIMS) instrument centered at 2.0 μm (5000 cm^{-1}), 1.6 μm (6250 cm^{-1}), and 1.3 μm (7692 cm^{-1}) are indicative of strong proportions of dark organics of hitherto undetermined chemical composition and origin (*7*). With a volume of three to seven times the organics of all of Titan's seas and lakes combined, these dark dunes represent the dominating surface sink of carbon in Titan's methane cycle (*8*). Since these dunes also control Titan's hydrocarbon balance and climate on a planetary scale, unraveling the origin and chemical pathways needed to form the organic dune material is vital not only to eventually understand Titan's chemical evolution but also to grasp how alike the chemistries on Titan and on Earth might have been like before life emerged on Earth 3.5 million years ago (*8*).

Planetary scientists proposed that these organics form in the atmosphere from methane (CH_4) and nitrogen (N_2) via solar photon–initiated molecular mass growth processes though reaction networks involving complex sets of gas phase ion—molecule and neutral—neutral reactions (*9*, *10*) of aromatic and resonantly stabilized free radicals such as phenyl (C_6H_5) and propargyl (C_3H_3), respectively, before eventually precipitating onto Titan's surface (*5*). However, in recent years, the hypothesis of participating atmospheric haze (*2*) has come under harsh scrutiny, since the material of the dark dunes in Shangri-La is defined by particle sizes of a few 100 μm (*6*), whereas the atmospheric aerosols are notably smaller, with diameters of only some 10 nm as established by the Synthetic Aperture Radar Imager (Cassini Orbiter) (*11*) and the Descent Imager/Spectral Radiometer (Huygens Lander) (*12*). The substantial discrepancy of these size distributions necessitates an alternative source of the dune material, implicating Titan's elusive surface chemistry (*13*).

Here, we show that polycyclic aromatic hydrocarbons (PAHs) such as naphthalene ($C_{10}H_8$) and phenanthrene ($C_{14}H_{10}$), along with its precursors (benzene, C_6H_6; phenylacetylene, C_6H_5CCH; styrene, $C_6H_5C_2CH_3$), can be synthesized via a cosmic ray–mediated nonequilibrium chemistry in low-temperature acetylene (C_2H_2) ices on Titan's surface and may act as a critical molecular feedstock to the organic dune material. Cassini's VIMS revealed the presence of solid acetylene via the 1.55-μm (6450 cm^{-1}) and 4.93-μm (2030 cm^{-1}) absorptions at Titan's low-albedo equatorial regions Shangri La and Fensal-Aztlan/Quivira but not in the higher-albedo equatorial area of Tui Regio (*14*). Since the low-albedo regions with acetylene ices match the location of Titan's dark dunes as observed by the Cassini Synthetic Aperture Radar Imager, acetylene has been suggested to be directly linked to the molecular makeup of Titan's dark dune material (*6*, *15*). The cosmic ray–driven surface chemistry can efficiently convert acetylene ices over geological time scales through molecular mass growth processes via benzene and naphthalene to even more complex PAHs on Titan's surface, thus eventually furnishing the molecular building blocks not only for Titan's organic dunes but also for organics on airless bodies in general, such as on Kuiper belt objects such as Makemake, revealing red-shifted spectra due to dark organic material on its surface (*16*).

The experiments were conducted in an ultrahigh vacuum surface science setup at pressures of a few 10^{-11} torr by exposing ices of acetylene (C_2H_2) and deuterated acetylene (C_2D_2) to energetic electrons at 5 K. These experiments simulate the processing of acetylene ices on Titan's surface by secondary electrons, which are generated via galactic cosmic rays (GCRs) over a time of up to 104 years (see the Supplementary Materials) (*15*). After the irradiation, the ices were warmed up to

[1]W. M. Keck Research Laboratory in Astrochemistry, University of Hawaii at Manoa, Honolulu, HI 96822, USA. [2]Department of Chemistry, University of Hawaii at Manoa, Honolulu, HI 96822, USA.
*Corresponding author. Email: ralfk@hawaii.edu

300 K [temperature programmed desorption (TPD)] to release the molecules into the gas phase. The chemical modifications of the ices and the occurrence of functional groups linked to aromatics were monitored in situ via Fourier transform infrared spectroscopy (FTIR; Nicolet 6700) and ultraviolet-visible (UV-vis) spectroscopy (Nicolet Evolution 300) (see Materials and Methods). During the TPD process, subliming molecules were ionized via vacuum UV (VUV) single-photon ionization (SPI), and individual isomers were selectively ionized by one- and two-photon resonance-enhanced multiphoton ionization (REMPI), followed by a mass-resolved detection of aromatic molecules in a reflectron time-of-flight mass spectrometer (ReTOF-MS). The exploitation of model ices—also called analog ices in the planetary science community—offers a substantiated methodology and the first step in untangling Titan's surface chemistry (*17*). Acetylene ices as detected in Titan's low-albedo equatorial region Shangri La were selected as a proxy to explore the proof of concept as to what extent aromatic molecules and PAHs, in particular, can be formed via interaction with ionizing radiation on Titan's surface and how these high-energy pathways define the level of molecular complexity of aromatics synthesized in these processes.

RESULTS

Infrared and UV-vis spectroscopy

The acetylene ices were monitored before, during, and after the irradiation via infrared (FTIR) and UV-vis spectroscopy (see Materials and Methods). In the infrared spectra of the irradiated acetylene ices, several small hydrocarbons (methane [CH_4], ethane [C_2H_6], ethylene [C_2H_4], vinylacetylene [C_4H_4], and diacetylene [C_4H_2]) and critical functional groups of PAHs were identified (Fig. 1A and table S1). Absorptions linked to PAHs comprise out-of-plane C—H deformation modes in substituted benzenes and aromatics [ν_{CH} (890 to 1100 cm^{-1})] along with aromatic CH stretching modes [ν_{CH} (3030 cm^{-1})] (*17*–*19*). Experiments with deuterium-labeled acetylene ices (C_2D_2) match the isotopic shifts determined for the out-of-plane C—H deformation [ν_{CD} (750 to 800 cm^{-1})] and aromatic CH stretching modes [ν_{CD} (2265 cm^{-1})] (fig. S1 and table S1) (*19*–*23*). These findings imply that functional groups connected with PAHs are the results of an exposure of the ices to the ionizing radiation at temperatures as low as 5 K. Similarly, UV-vis spectroscopy of the irradiated ices revealed a featureless increase of the absorption over the entire wavelength range from 190 to 1100 nm, which was most pronounced in the 190- to 400-nm region (Fig. 1B). Aromatic molecules such as benzene (C_6H_6), phenylacetylene (C_8H_6), styrene (C_8H_8), naphthalene ($C_{10}H_8$), and phenanthrene ($C_{14}H_{10}$) hold strong $\pi \rightarrow \pi^*$ absorptions in this region of the electromagnetic spectrum (Fig. 2) (*24*).

After the irradiation phase, we carried out TPD studies where each ice was heated at a rate of 0.5 K min^{-1} to 300 K while simultaneously monitoring the ices spectroscopically. The infrared and UV-vis data both revealed changes that correlate with aromatic products formed at 5 K but not during TPD. For example, in the FTIR, a peak was observed to increase in intensity at 3030 cm^{-1} only during irradiation and then was observed to remain at constant intensity during TPD until almost 80 K, when its intensity began to decrease (fig. S2). Recall that FTIR is not selective for complex molecules and likely has multiple contributors; therefore, the initial decrease in intensity can be correlated with the sublimation of vinylacetylene (C_4H_4), while the remaining signal corresponds well with the sublimation event of benzene (C_6H_6) as detected via REMPI-ReTOF-MS. These assignments are also supported via the UV-vis spectra, which show no change in intensity of the UV-vis signal below 260 nm and only a gradual increase in intensity above 260 nm during TPD from 5 to 70 K (Fig. 2A). The latter is due to a change in the phase of the acetylene ice from amorphous to crystalline, which is further corroborated by the notable change in intensity between the 70 and 80 K spectra, where the phase change of acetylene occurs (*25*). The UV-vis spectra after 80 K still show absorptions, and these can only be due to products; the benzene molecule has an absorption of about 195 nm (Fig. 2C), and there is an increase in intensity at this wavelength after irradiation relative to the unirradiated acetylene spectrum (Fig. 2A). Although the intensity at 195 nm does increase between 5 and 90 K, this can be explained via a change in absorption cross section as, similar to acetylene, benzene changes from its amorphous state to a crystalline phase at about 90 K, which results in an increase in absorption cross section in the UV-vis regime (*26*). This change in the cross section [43.0 ± 0.5 megabarn (Mb), 25 K; 53 ± 0.5 Mb, 90 K] corresponds to the change in signal intensities (0.905 ± 0.005, 5 K; 1.151 ± 0.005, 90 K), and this explanation also agrees with the FTIR data that showed no increase in benzene-related peaks during TPD (fig. S2). These assignments are further substantiated by comparing the change in, for instance, the UV-vis spectra (Fig. 2) with the sublimation profile of potential aromatic molecules as determined mass spectroscopically via SPI-ReTOF-MS and REMPI-ReTOF-MS (Figs. 3 and 4). For example, the 195-nm feature, potentially related to benzene (C_6H_6) decreases in intensity from 100 to 220 K (Fig. 2B), while the ion counts at mass-to-charge ratio (*m/z*) indicative of benzene (*m/z* = 78) can be simultaneously observed from 120 to 210 K in the gas phase (Figs. 3 and 4). Similar correlations are readily visible for phenylacetylene (C_8H_6), styrene (C_8H_8), and naphthalene ($C_{10}H_8$) in the range of 190 to 295 nm and for phenanthrene ($C_{14}H_{10}$) from 260 to 380 nm over the temperature range of 220 to 280 K. However, the lack of sensitivity of FTIR and UV-vis only allows for a tentative assignment to these molecules, and other methods are necessary to uniquely identify the products.

Consequently, the infrared and UV-vis analysis exposes the existence of functional groups during the irradiation of the ices such as out-of-plane C—H/C—D deformation and aromatic C—H/C—D stretching modes along with delocalized (aromatic) π-electronic systems present in (substituted) benzenes and in PAHs. Since these functional groups emerge during the irradiation, but not during the TPD phase, the aromatic molecules are synthesized at 5 K as the result of the radiation exposure but not through thermal processing of the irradiated ice. Recognizing that the fundamentals of PAHs such as naphthalene and phenanthrene fall in the same range of the electromagnetic spectrum and hence overlap, neither infrared nor UV-vis spectroscopy permits an identification of specific PAHs (*20*–*23*, *27*). In other words, functional groups are not unique to individual PAHs and do not pinpoint any particular molecule. For that reason, complementary analytical techniques are essential to identify distinct aromatic molecules and PAHs in particular.

SPI-ReTOF-MS and REMPI-ReTOF-MS

To identify discrete molecular species, we used photoionization ReTOF-MS (PI-ReTOF-MS) during the TPD phase. This approach signifies a unique method to identify gas phase molecules isomer selectively after photoionization based on their discrete ionization energies (IEs; SPI-ReTOF-MS) (*28*) or with the aid of distinct resonance lines (REMPI-ReTOF-MS) (*29*). First, exploiting a photon energy of 10.49 eV (λ = 118.152 ± 0.001 nm), we analyzed the entire range of

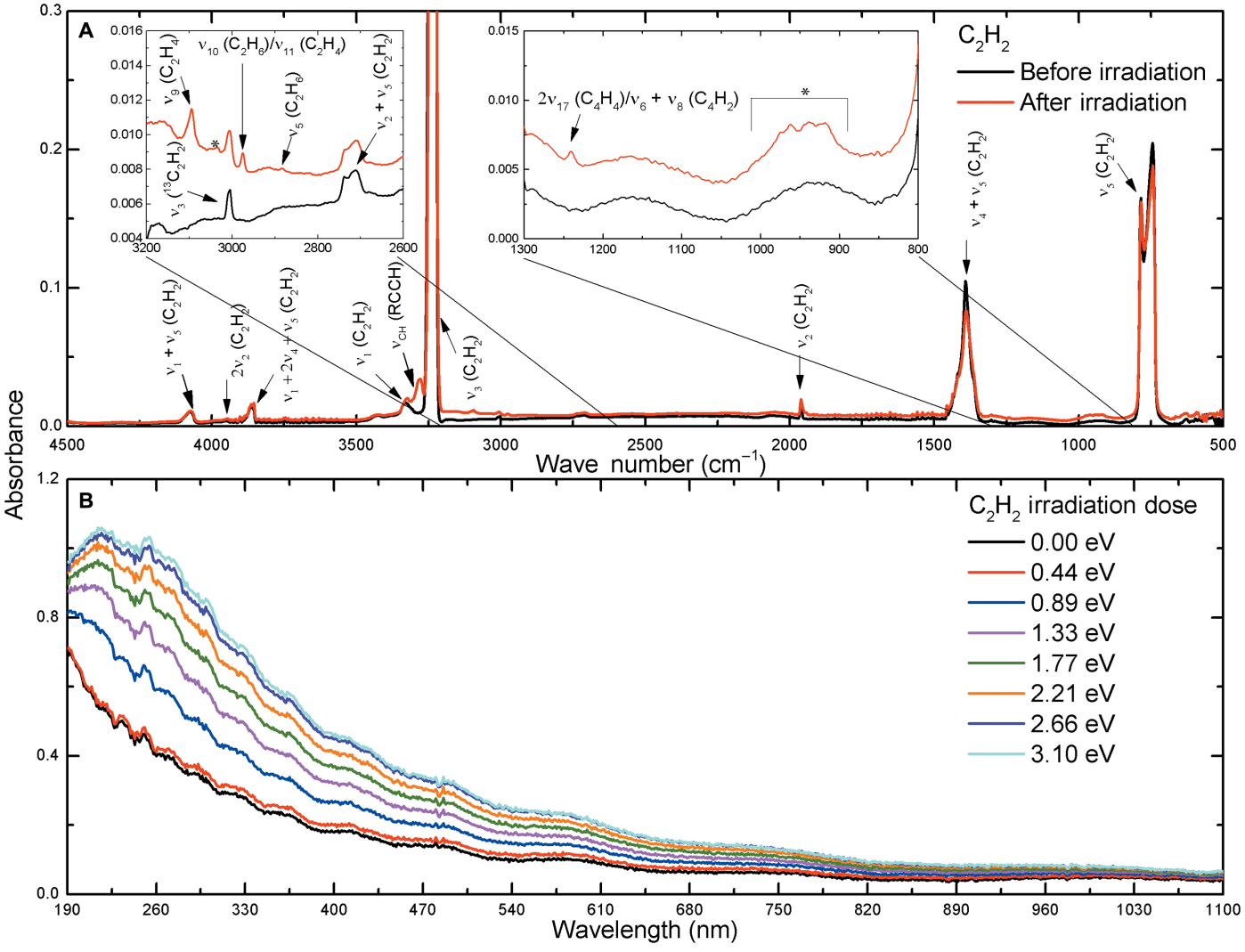

Fig. 1. Acetylene ice spectra before and after processing with energetic electrons. (**A**) FTIR spectra from 500 to 4500 cm^{-1} with 2600 to 3200 cm^{-1} magnified by 25× (left), with 800 to 1300 cm^{-1} magnified by 20× (right), and PAH-related features identified with asterisks (*) (table S2). (**B**) UV-vis spectra from 190 to 1100 nm with new features at lower wavelengths appearing.

subliming products, as hydrocarbons hold adiabatic IEs below 10.49 eV (Fig. 3A). Ion signals at *m/z* = 78 ($C_6H_6^+$), 102 ($C_8H_6^+$), 104 ($C_8H_8^+$), 128 ($C_{10}H_8^+$), and 178 ($C_{14}H_{10}^+$) could correspond to benzene (IE = 9.244 ± 0.001 eV), phenylacetylene (IE = 8.825 ± 0.001 eV), styrene (IE = 8.464 ± 0.001 eV), naphthalene (IE = 8.144 ± 0.001 eV), and phenanthrene (IE = 7.891 ± 0.001 eV), along with anthracene (IE = 7.439 ± 0.006 eV), respectively, since each of these molecules can be photoionized at 10.49 eV (Fig. 4) (*24*). However, it is important to highlight that each of these aromatic molecules has multiple isomers, which can also be ionized at 10.49 eV; for instance, recent electronic structure calculations revealed the existence of 217 isomers of benzene, of which some isomers have adiabatic IEs (*30*). Therefore, the overlap of distinct IEs of multiple isomers complicates the assignment of individual C_6H_6, C_8H_6, C_8H_8, $C_{10}H_8$, and $C_{14}H_{10}$ isomers using SPI-ReTOF-MS.

REMPI represents an elegant tool to overcome the aforementioned limitations to ultimately identify the carriers of the ion signal at *m/z* = 78 ($C_6H_6^+$), 102 ($C_8H_6^+$), 104 ($C_8H_8^+$), 128 ($C_{10}H_8^+$), and 178 ($C_{14}H_{10}^+$). Here, REMPI first accesses an excited intermediate state, which is characteristic for the individual isomer to be identified, via a resonant photon absorption followed by a second photon, which then ionizes the molecule (*29*). The resonance lines were experimentally determined for each aromatic molecule investigated (Fig. 4). As a typical example, Fig. 3 (A and B) compares the SPI-ReTOF-MS and the REMPI-ReTOF-MS obtained at 10.49 eV and via [1+1] REMPI at 4.787 eV for benzene (C_6H_6). Using SPI (Fig. 3A), the molecular parent ion of vinylacetylene at *m/z* = 52 ($C_4H_4^+$) dominates the spectrum, whereas exploitation of the [1+1] REMPI scheme characteristic for benzene yields maximum ion counts at *m/z* = 78 ($C_6H_6^+$) (Fig. 3B). To identify individual aromatic molecules, one-color [1+1] REMPI schemes are exploited, which are isomer specific for benzene (λ = 258.994 ± 0.001 nm, 4.787 eV), phenylacetylene (λ = 278.801 ± 0.001 nm, 4.447 eV), styrene (λ = 287.202 ± 0.001 nm, 4.317 eV), and naphthalene (λ = 278.600 ± 0.001 nm, 4.450 eV) (Figs. 3 and 4). A comparison of the SPI and REMPI-ReTOF-MS TPD profiles recorded at *m/z* = 78 ($C_6H_6^+$) and 102 ($C_8H_6^+$) reveals that benzene and phenylacetylene are the major contributors (Fig. 4, A and B) (*29*, *31*). The differences between the SPI and REMPI sublimation profiles for *m/z* = 78 and 102 can be

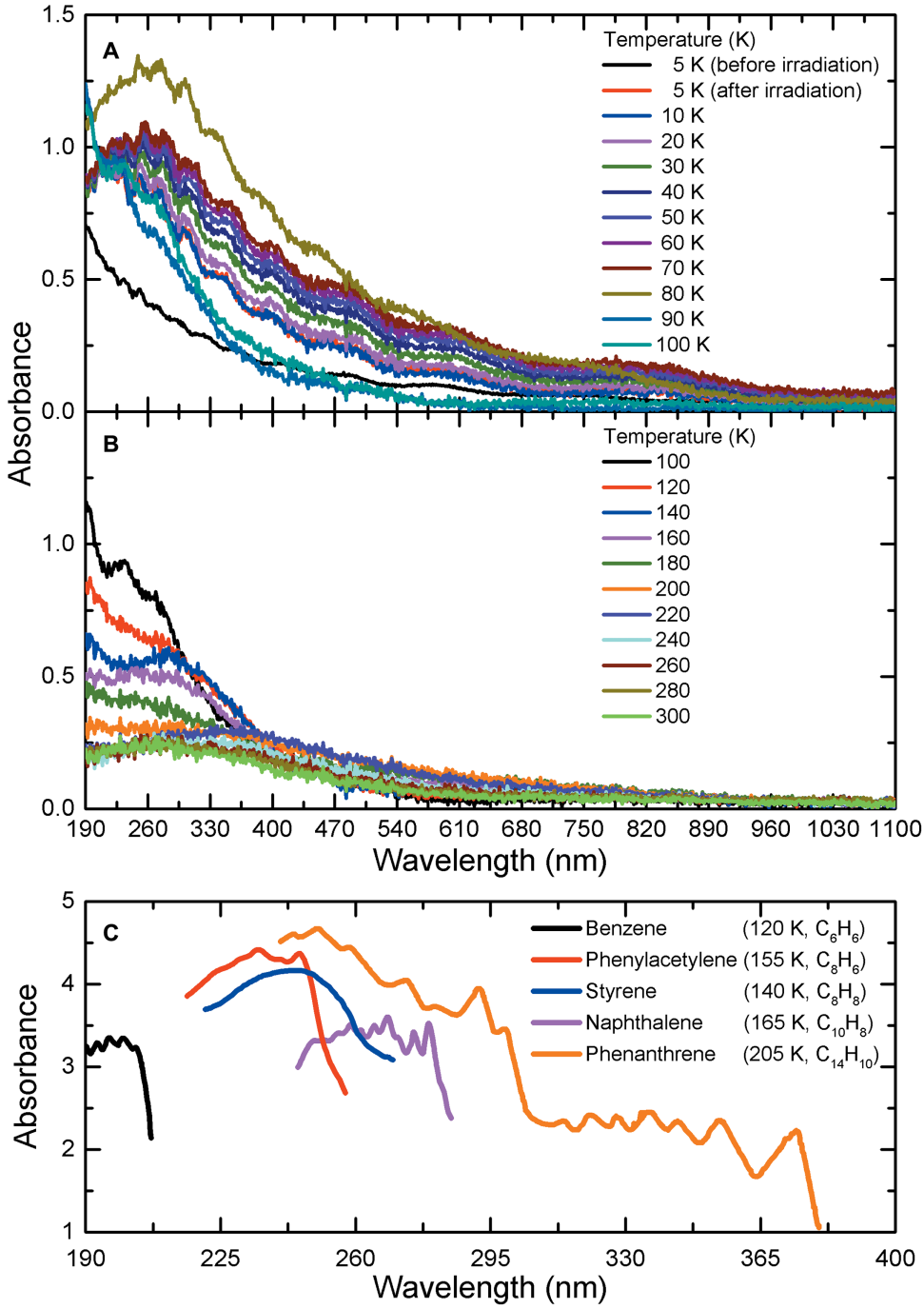

Fig. 2. UV-vis spectra from 190 to 1100 nm during TPD from 5 to 300 K. (**A**) Spectra from 5 to 100 K and (**B**) 100 to 300 K in the UV-vis with changes in features possibly corresponding to aromatic molecules (see main text for details). (**C**) Reference spectra from the National Institute of Standards and Technology for each of these possible contributors with experimentally determined sublimation onset temperatures noted in the legend.

correlated with the ionization of additional C_6H_6 and C_8H_6 isomers using SPI, which cannot be ionized while exploiting REMPI. One-color REMPI experiments also presented compelling evidence on the formation of styrene (C_8H_8) (Fig. 4C) and naphthalene ($C_{10}H_8$) (Fig. 4D). Here, a detailed comparison of the SPI and REMPI data revealed that besides styrene and naphthalene, additional isomers are formed since the TPD profiles for the SPI and REMPI data only match in the low-temperature regimes covering about 140 to 200 K and 160 to 225 K for styrene and naphthalene, respectively. To probe the synthesis of phenanthrene ($C_{14}H_{10}$) and anthracene ($C_{14}H_{10}$), we used both one- and two-color REMPI schemes (Fig. 4, E and F) and identified phenanthrene; anthracene could not be detected (see Materials and Methods). The two-color REMPI scheme ($\lambda_1 = 341.054 \pm 0.001$ nm, 3.635 eV; $\lambda_2 = 287.202 \pm 0.001$ nm, 4.317 eV) is isomer specific for phenanthrene,

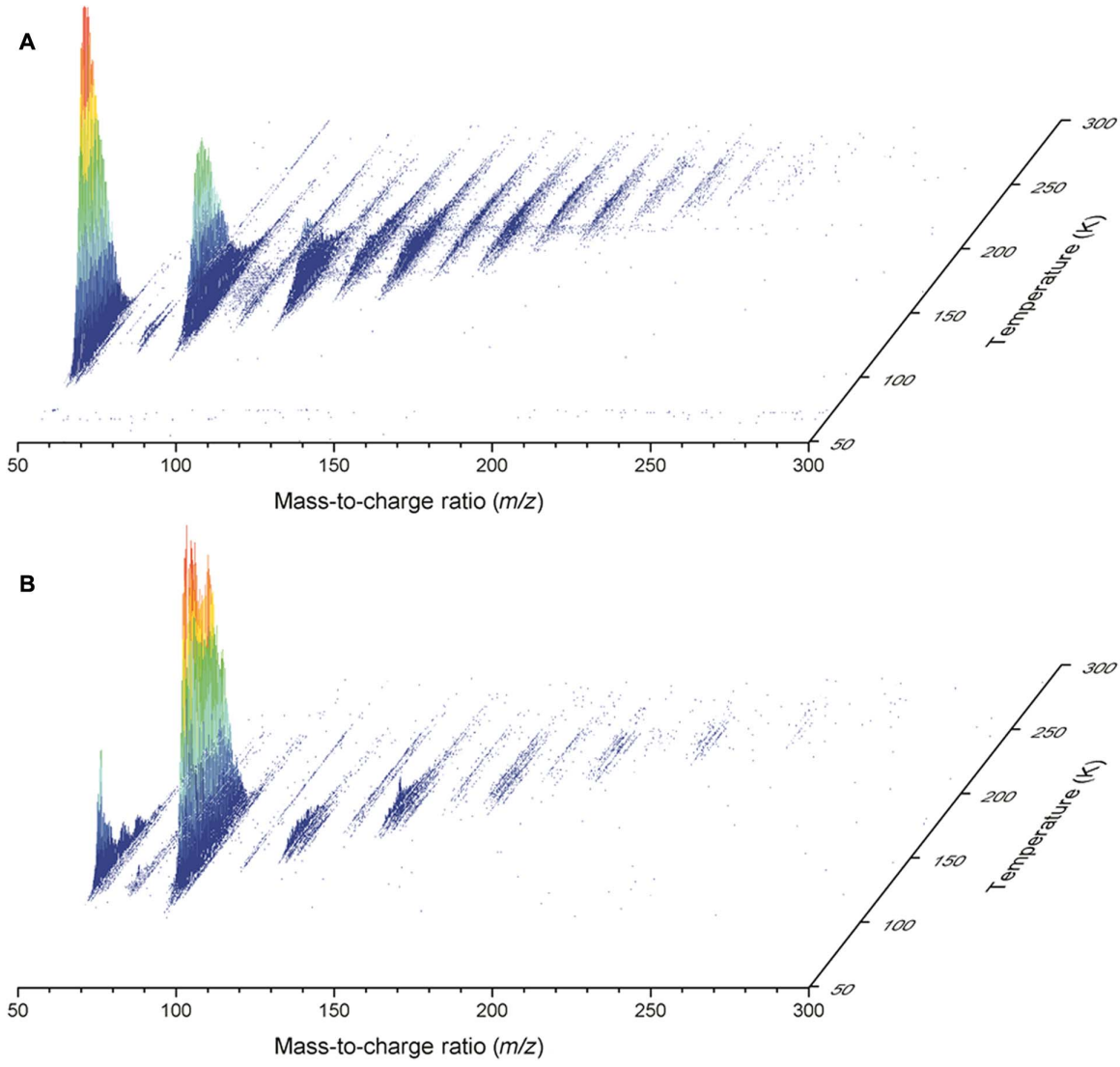

Fig. 3. Temperature-dependent PI-ReTOF-MS spectra of the subliming molecules from the exposed acetylene ices. (**A**) SPI at 118.152 nm (10.49 eV) used to ionize most subliming molecules. (**B**) REMPI at the resonance wavelength of 258.994 nm (4.787 eV) to isomer to specifically identify benzene.

while the one-color process (λ = 282.033 ± 0.001 nm, 4.396 eV) is not isomer specific between anthracene and phenanthrene, as both isomers have an absorption in this region. However, the one-color REMPI scheme accesses a more intense resonance line of phenanthrene, relative to the two-color REMPI transition for phenanthrene and compared to anthracene's one-color REMPI transition, and therefore produces a stronger signal, but this could also have some contributions from anthracene (*32*, *33*). Note that larger PAHs were also ionized and detected using [1+1] REMPI (λ = 258.994 ± 0.001 nm, 4.787 eV) due to their broad absorptions in this region. On the basis of the ion signals up to m/z = 260 (Fig. 3B), pyrene ($C_{16}H_{10}^+$, m/z = 202), which holds four six-membered rings, along with its isomers, is the most complex PAH synthesized in the present experiments (table S2).

In summary, the REMPI-ReTOF-MS data provide conclusive evidence on the formation and detection of five individual aromatic molecules: benzene, phenylacetylene, styrene, naphthalene, and phenanthrene. Since the photoionization cross sections of these molecules at 10.49 eV are available, we can also extract their yields and branching ratios (table S3). Here, the production yields for benzene, phenylacetylene, styrene, naphthalene, and phenanthrene were calculated to be 3.72 ± 1.30 × 10^{-3}, 4.66 ± 1.63 × 10^{-4}, 2.74 ± 0.96 × 10^{-4}, 1.58 ± 0.55 × 10^{-4}, and 1.18 ± 0.41 × 10^{-5} molecules eV^{-1}, respectively (Fig. 5). These yields correspond to a ratio of 314 ± 110:39 ± 14:23 ± 8:13 ± 5:1 ± 0.4 for benzene, phenylacetylene, styrene, naphthalene, and phenanthrene, respectively, with benzene being the most abundant aromatic molecule holding yields close to one order of magnitude higher than each of the remaining aromatic molecules identified. When successively adding benzene rings, the yields drop from benzene via naphthalene to phenanthrene by about one order of magnitude each, suggesting a mechanism involving a stepwise mass growth of PAHs in acetylene ices during the radiation exposure.

DISCUSSION

Having firmly ascertained that (polycyclic) aromatic hydrocarbons can be easily formed in acetylene ices upon interaction with ionizing

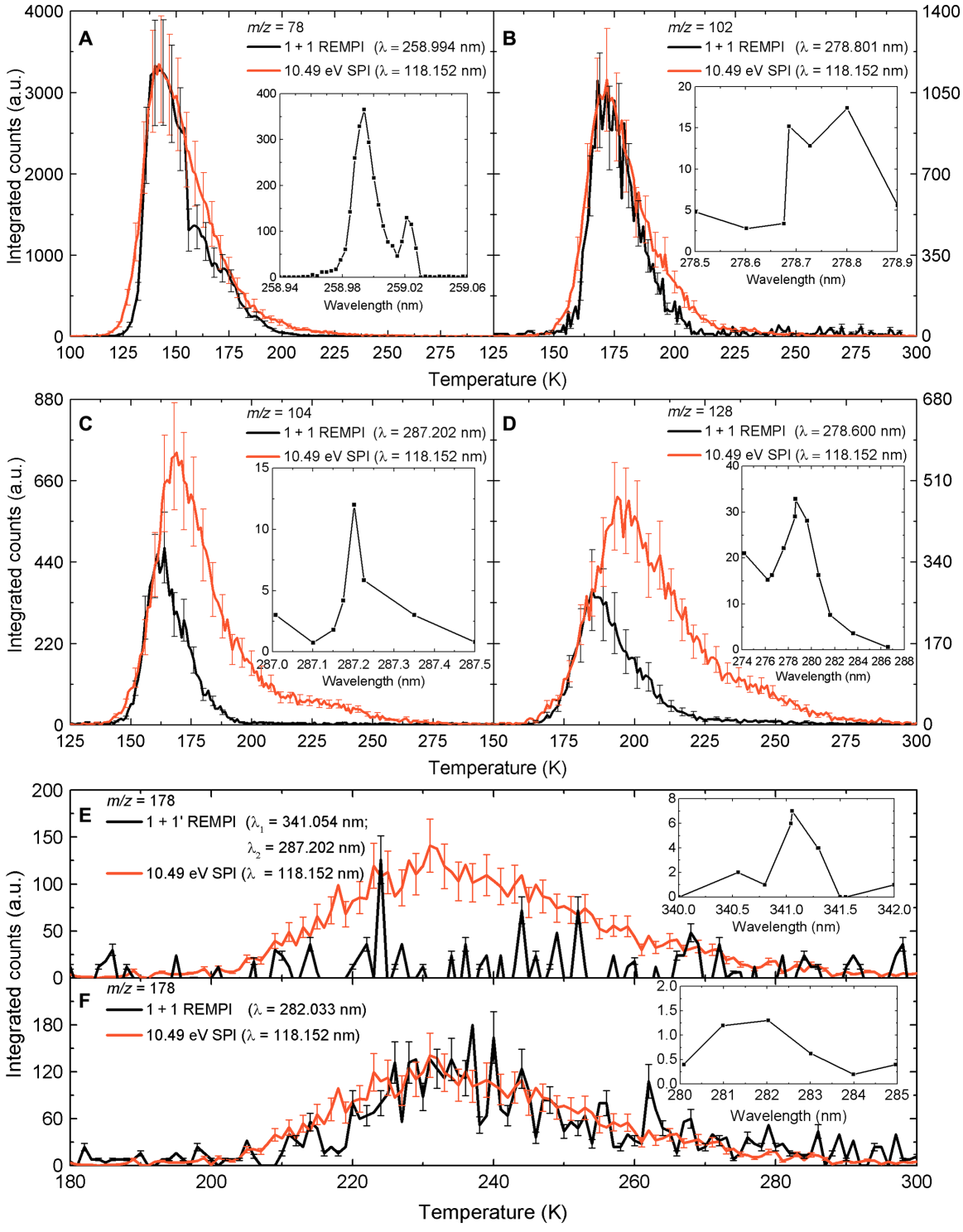

Fig. 4. Overlay of SPI (red) and REMPI (black) ion signals versus temperature for benzene, phenylacetylene, styrene, naphthalene, and phenanthrene with insets displaying the REMPI wavelength dependence. (**A**) *m/z* = 78 (benzene). a.u., atomic mass units. (**B**) *m/z* = 102 (phenylacetylene). (**C**) *m/z* = 104 (styrene). (**D**) *m/z* = 128 (naphthalene). (**E**) and (**F**) *m/z* = 178 (phenanthrene). Error bars indicate 20% (SD).

radiation via molecular mass growth processes involving ring annulation, we are transferring our finding now from the laboratory to the "real" astrophysical environments—the surface of Saturn's moon Titan. This is critical since laboratory simulation experiments cannot replicate all chemical and physical conditions in Solar System ices simultaneously, with the ices containing diverse molecules and the GCRs interacting with Titan's surface ices with a wide range of high energies (see the Supplementary Materials). The low temperature of Titan's surface of 94 K

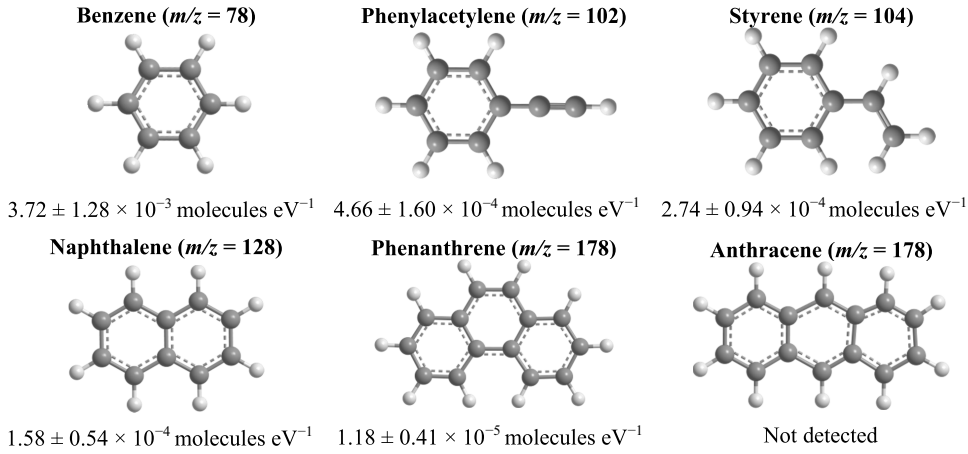

Fig. 5. Structures of PAH isomers was searched via REMPI along with their production yields. Error bars indicate 35% (SD).

inhibits reactions under thermal equilibrium, which have large entrance barriers (or classical activation energies). Although the overall reactions to form the three simplest aromatic species, benzene, naphthalene, and phenanthrene [reactions (1) to (3)], on the singlet ground-state surface are strongly exoergic by up to 583 kJ mol^{-1}, a notable entrance barrier of 140 kJ mol^{-1} blocks the very first step of the reaction sequence involving two acetylene molecules leading to C_4H_4 reaction intermediates (*17*). Consequently, the synthesis of aromatic molecules from acetylene on Titan's surface cannot be initiated under thermodynamic equilibrium but must involve nonequilibrium processes, which impart sufficient energy into the transition state of the reaction to overcome the barrier to reaction. This can be achieved by transferring part of the kinetic energy of the secondary electrons to the acetylene molecule(s), leading to electronically excited acetylene such as in the a^3B_2 or a^3A_u states, which lie 308 and 397 kJ mol^{-1} above the electronic ground state while penetrating the ices (*17*). Electronically excited acetylene may react with a neighboring singlet acetylene molecule to form a triplet C_4H_4 reaction intermediate via a barrier of only 4 kJ mol^{-1}, which can be easily overcome by, for instance, vibrational energy in one of the reactants (*17*). Similar mechanisms highlighting the critical role of electronically excited acetylene (*34*) and ethylene (*28*) were found in the reactions with carbon monoxide (CO) leading to cyclopropenone (C_2H_2CO) and cyclopropanone (C_2H_4CO), respectively. Therefore, upon reaction of triplet C_4H_4 with a third acetylene molecule, triplet benzene can be formed, which undergoes facile intersystem crossing to the singlet benzene. Analogous molecular mass growth processes via electronically excited (triplet) reactants may lead even to naphthalene and phenanthrene on Titan's surface. The molecular mass growth process via ring annulation is also supported by the diminished yields of benzene to naphthalene to phenanthrene of 3.72 ± 1.30 × 10^{-3}, 1.58 ± 0.55 × 10^{-4}, and 1.18 ± 0.41 × 10^{-5} molecules eV^{-1}, respectively, as the number of benzene rings increases from one via two to three at doses up to 3.1 ± 0.3 eV per molecule. Preliminary qualitative studies of PAHs formed by exposing acetylene ices to ionizing radiation at 10 K revealed that an increase of the dose by a factor of about 10 to 27 ± 2 eV per molecule promotes the synthesis of even more complex aromatics such as chrysene ($C_{18}H_{12}$), perylene ($C_{20}H_{12}$), pentacene ($C_{22}H_{14}$), and coronene ($C_{24}H_{12}$), carrying up to six benzene rings (*19*). Therefore, once a PAH is formed, the (electronically excited) PAH may gain another six-membered ring by successive reactions with two (electronically excited) acetylene molecules. These findings support the proposed reaction mechanism of a stepwise mass growth through successive ring annulation as the dose increases. The transition from benzene to naphthalene and phenanthrene (Fig. 5), along with potentially higher molecular weight products (table S2), via nonequilibrium reactions likely involving excited (triplet) states of the reactants in low-temperature ices defines a critical, hitherto ignored reaction class for the build-up of complex PAHs through stepwise molecular mass growth processes on Titan's surface

$$3C_2H_2(X^1\Sigma_g^+) \rightarrow C_6H_6(X^1A_{1g}) + H_2(X^1\Sigma_g^+) \quad \Delta_R G = -583 \text{ kJ mol}^{-1} \quad (1)$$

$$C_6H_6(X^1A_{1g}) + 2C_2H_2(X^1\Sigma_g^+) \rightarrow C_{10}H_8(X^1A_g) + H_2(X^1\Sigma_g^+) \quad \Delta_R G = -405 \text{ kJ mol}^{-1} \quad (2)$$

$$C_{10}H_8(X^1A_g) + 2C_2H_2(X^1\Sigma_g^+) \rightarrow C_{14}H_{10}(X^1A_1) + H_2(X^1\Sigma_g^+) \quad \Delta_R G = -404 \text{ kJ mol}^{-1} \quad (3)$$

Last, it should be highlighted that the present studies were conducted in the condensed phase (ices) but not under single-collision conditions in the gas phase (*35*). Consequently, it is not achievable to determine the efficiency of each elementary step involved in the mass growth processes leading to individual aromatic molecules. This necessitates pulse-probe experiments with femtosecond (few 10-fs pulses) electron pulses penetrating the ice sample; these setups do not exist as of today. Nevertheless, we propose that the present study is a critical template to expand further investigations on the formation of aromatic structures and their molecular mass growth processes on Titan's surface via GCR-mediated nonequilibrium surface chemistry and their contribution to the dark material of Titan's dunes. Here, Titan's nitrogen-rich atmosphere also leads to the production of hydrogen cyanide, which may sequester similarly to acetylene to Titan's surface. GCR processing of hydrogen cyanide–bearing acetylene ices will couple Titan's nitrogen and hydrocarbon chemistries, likely leading to nitrogen-based PAHs (NPAHs) such as (iso)quinoline and possibly biorelevant NPAHs such as adenine ($C_5H_5N_5$).

Summary

To conclude, our experimental study identified in situ benzene, phenylacetylene, styrene, naphthalene, and phenanthrene as key aromatic reaction products formed upon interaction of ionizing radiation with low-temperature acetylene ices in an attempt to simulate the interaction of high-energy GCRs with organics on Titan's surface. Since the reactions of singlet acetylene involve substantial entrance barriers, these processes must be initiated under nonequilibrium conditions to overcome the barriers to reaction involving electronically excited molecules. The elucidated GCR-mediated pathways to aromatics reveal a facile, previously ignored synthetic route for the formation of PAHs via molecular mass growth processes through stepwise ring annulation, which may lead to even more complex PAHs such as coronene ($C_{24}H_{12}$) (*19*). This nonequilibrium chemistry is critical to Titan's surface chemistry considering its low temperature of only 94 K, which precludes chemical reactions of acetylene under thermal equilibrium. While most of the energy sources are absorbed by Titan's thick atmosphere, energetic GCRs are capable of penetrating through the atmosphere and depositing energy into Titan's surface. As the GCRs penetrate the surface of Titan, they produce secondary electrons that can cause chemical processing of the surface organics. Here, the processing of a model acetylene ice at 5 K with energetic electrons, which mimics the secondary electrons produced by GCRs, proves the concepts that GCRs could initiate a complex chemistry on Titan's surface. Although the temperature in the simulation experiments is lower than Titan' actual surface temperature, this proof-of-concept study provides a fundamental understanding of the nonequilibrium, temperature invariant chemical pathways available in acetylene ice that are capable of taking place on Titan. With acetylene ices identified in Titan's low-albedo equatorial regions (*14*) and GCR fluxes valued in the range of 6.2×10^8 to 6.2×10^9 eV cm^{-2} s^{-1} on Titan's surface (*15*, *36*, *37*), our simulation experiments mimic Titan's surface chemistry over a range of 10.4 to 104 years using the higher and lower bounds, respectively. Therefore, this study reveals that even over a relatively short time scale of about 104 years, PAHs as complex as phenanthrene can be synthesized on Titan's surface. Those PAHs carrying up to three benzene rings such as phenanthrene ($C_{14}H_{10}$) are colorless (white) but can undergo further molecular mass growth processes to yellowish coronene ($C_{24}H_{12}$) over 14,000 years (*19*) and potentially via black dicoronylene ($C_{48}H_{20}$) to graphitic type structures (*38*) over geological time scales of 2×10^8 years and act as potential building blocks—at least in part—of Titan's dark dunes. Consequently, our simulation study implies that the GCR-triggered transformation of acetylene via benzene—the simplest aromatic molecule detected on Titan's surface (*39*)—is one of the most fundamental processes of the context of the chemical evolution of planetary surfaces, thus defining the level of molecular complexity of aromatics synthesized in these processes. These findings ultimately change our perception that PAHs can be solely formed in the atmosphere of hydrocarbon-rich planets and their moons via hydrogen abstraction–acetylene addition (*40*) and hydrogen abstraction–vinylacetylene addition (*41*) type reactions, followed by precipitation to the surface, as believed previously not only for Titan but also for our Solar System in general.

Therefore, the facile, GCR-mediated synthesis of PAHs in low-temperature acetylene ices represents a fundamental shift from currently accepted perceptions leading to PAH formation in hydrocarbon-rich atmospheres of planets and their moons, followed by their precipitation to the ground (*4*). The versatile concept of PAH synthesis in acetylene ices has vital implications to the surface chemistry and interpretation of reflection spectra of airless bodies, on which either hydrocarbon ices were detected such as Makemake or which reveal areas of lower albedos proposing "dark organic surface material" of hitherto unknown origin and composition such as on Hyperion, Iapetus, and Phoebe (*42*, *43*), throughout our Solar System. Cassini's VIMS observations of "dark material" on Phoebe and Iapetus revealed absorption in the spectral range of 3.0 to 3.6 μm, centered at 3.29 μm, which was assigned to C—H stretching modes of PAHs (*44*, *45*). Similarly, the surfaces of Jupiter's moon Ganymede and more weakly on Callisto show evidence related to dark organics (*46*). In addition, the New Horizons mission revealed that Pluto's dark regions, as well as the dark areas of Charon, Nix, and Hydra, can be matched with organics related to Titan's organic inventory and have been suggested to be due to complex hydrocarbons among them PAHs (*47*, *48*). Further dark organic-containing objects include the dwarf planet Ceres in its Occator region via a 3.4-μm absorption band characteristic of organics, as well as Sedna, 2006 SQ372, and 2000 OO67, which have been described as "very" or "ultra" red objects associated with dark organics produced from surface irradiation; recently, the surface of comet 67P/Churyumov-Gerasimenko was exhibited to have a darker surface than average possibly due to organic material (*49*, *50*). Last, an interesting parallel to Titan is the Kuiper belt object Makemake, observed with the Keck telescope at 1.4 to 2.5 μm, revealing features related to acetylene ice on its surface and a dark surface characterized as complex hydrocarbons possibly containing aromatics (*16*). Obviously, on airless bodies such as Makemake, PAHs cannot originate from atmospheric precipitation, and the present findings of a GRC-triggered formation and complexation of PAHs from acetylene strongly reinforces that these dark organics are likely produced via surface processes. This effect is amplified by the detection of methane (CH_4) ices on outer Solar System bodies, which can be easily converted by ionizing radiation to acetylene (*16*, *51*–*53*) thus presenting a versatile, previously disregarded mechanism leading to the formation of PAHs on the hydrocarbon-rich surfaces of planets and their moons in our Solar System.

MATERIALS AND METHODS

Experimental

The experiments were carried out in an UHV chamber operated at base pressures of a few 10^{-11} torr (*54*). A highly reflective silver mirror coated with rhodium is interfaced to a closed-cycle helium refrigerator exploiting indium foil to ensure thermal conductivity; this system is positioned inside the UHV chamber and can be rotated in the horizontal plane or translated vertically. After the substrate was cooled to 5.0 ± 0.1 K, acetylene (C_2H_2, >99.9%, Airgas) was deposited onto the substrate using a glass capillary array. Traces of acetone (CH_3COCH_3) were eliminated quantitatively from the acetylene by using a dry ice–ethanol slush bath (200 K) to freeze only the acetone but not the acetylene. The growth of the ice was monitored online and in situ via interferometry by reflecting a HeNe laser (λ = 632.8 nm; 25-LHP-230, CVI Melles Griot) off of the silver mirror into a photodiode (*55*, *56*); with a refractive index (*n*) of 1.34 for solid acetylene, the thickness was calculated to be 750 ± 60 nm (*25*). Similarly, isotopically labeled D2-acetylene (C_2D_2, 99% + D; CDN Isotopes) ices of similar thickness (780 ± 60 nm) were processed to confirm both infrared spectroscopy and MS assignments via the observed isotopic shifts. Each ice was monitored spectroscopically via an FTIR (4500 to 500 cm^{-1}; resolution, 4 cm^{-1}) spectrometer (Nicolet 6700) and a UV-vis (1100 to 190 nm; resolution, 4 nm) spectrometer (Nicolet Evolution 300) to probe the vibrational modes and electronic transitions,

respectively, of molecules in the sample, online and in situ before, during, and after processing. Concurrently, the incident light of the UV-vis spectrometer reflected off of the rhodium-coated silver mirror at an angle of 30° and was focused onto a photodiode detector that is isolated from ambient light. Rhodium coating was critical, because in this wavelength regime, the silver substrate absorbs at 320 nm (*57*).

To process the acetylene ices, energetic electrons (5 keV; SPECS EQ 22/35) simulating secondary electrons formed in the track of GCRs penetrating the ice (*58*) were directed at 1.0 ± 0.1 cm^2 of the acetylene ice, at an incidence angle of 70° relative to the surface normal of the mirror, for 45 min at a current of 30 nA (see the Supplementary Materials). The average penetration depth of the impinging electrons was calculated to be 370 ± 40 and 310 ± 30 into the acetylene (C_2H_2) and D2-acetylene (C_2D_2) ices, respectively, using the known density of acetylene (C_2H_2, ρ = 0.76 ± 0.08 g cm^{-3}; C_2D_2, ρ = 0.89 ± 0.09 g cm^{-3}) from Monte Carlo simulations via CASINO 2.42 software (*59*–*61*). Here, the electrons were calculated to deliver average doses of 3.1 ± 0.3 and 3.4 ± 0.3 eV per molecule into the acetylene (C_2H_2) and D2-acetylene (C_2D_2) ices, respectively (table S3). In addition, a control experiment under identical conditions was performed but with no irradiation of the acetylene or D2-acetylene ice. These experiments revealed that no ion peaks from nonirradiated acetylene ice with the ion signals of interest at *m/z* = 78, 102, 104, 128, or 178 were present (fig. S3).

After the irradiation phase, the ices were warmed up to 300 K at a rate of 0.5 K min^{-1} (TPD) while monitoring the ices with both FTIR and UV-vis spectroscopy simultaneously. The subliming molecules were analyzed after photoionization via the SPI-ReTOF-MS and REMPI-ReTOF-MS. SPI uses nonresonant four-wave mixing by frequency tripling the third harmonic (354.456 nm) of an Nd:YAG laser in pulsed gas jets of xenon. This results in the production of VUV light with an energy of 10.49 eV (118.152 nm). The VUV light is then separated from other wavelengths with biconvex lithium fluoride lens and focused in front of the substrate to use a single photon to ionize the subliming molecules. The ionized molecules were detected using a modified ReTOF-MS (Jordan TOF products Inc.). Here, the ReTOF-MS detects the ions via a multichannel plate within the dual chevron configuration; this signal was then amplified (Ortec 9305) and shaped using a 100-MHz discriminator. Using 4-ns bin widths and 3600 sweeps via a multichannel scaler (FAST ComTec, P7888-1 E) triggered at 30 Hz (Quantum Composers, 9518), the resulting spectra were recorded. This setup corresponds to a single mass spectrum per 1 K change in temperature of the substrate. Alternatively, one- and two-color REMPI was exploited to photoionize the subliming molecules. Here, the UV light was produced by pumping a dye laser with an Nd:YAG laser to produce visible light, which was then frequency doubled or tripled using β-barium borate crystals to produce UV photons of a well-defined wavelength (±0.001 nm). To confirm that the setup was capable of performing a REMPI analysis of individual molecules, carbon monoxide (CO) was used to calibrate the system (fig. S4). Using a one-color three-photon process [2+1] (*62*), carbon monoxide (CO) was ionized and detected in the gas phase. Here, to reach the intermediate excited level of carbon monoxide ($B^1\Sigma^+$, 10.78 eV), two photons were needed; the third photon ionized the excited carbon monoxide molecule. In addition, a carbon monoxide ice was prepared on the cooled substrate and subjected to TPD under same conditions as in the acetylene experiment. During sublimation, the wavelength was scanned from 230.00 to 230.15 nm to confirm the resonant wavelength needed for the most efficient ionization of carbon monoxide. Once this wavelength was determined, the experiment was repeated by subliming carbon monoxide ice but holding the REMPI wavelength constant on the maximum wavelength determined from the scan experiment (fig. S4). For the detection of benzene, phenylacetylene, styrene, naphthalene, and phenanthrene, a one-color two-photon process [1+1] was used. Each REMPI study was completed twice. First, the wavelength corresponding to the REMPI literature values for each molecule were scanned over to confirm the wavelength at which maximum ionization occurred (benzene, 258.994 nm; phenylacetylene, 278.801 nm; styrene, 287.202 nm; naphthalene, 278.600 nm; and phenanthrene, 282.033/341.054 nm); these data compare very well to literature values of 258.986, 278.7, 287.4, 278.6, and 282.5/341.0 nm for benzene, phenylacetylene, styrene, naphthalene, and phenanthrene, respectively (*29*, *31*–*33*, *63*, *64*). Next, each REMPI experiment was repeated holding the wavelength at the maximum REMPI wavelength signal detected from the wavelength scan. Last, a two-color two-photon [1+1] REMPI scheme was used to confirm the presence of phenanthrene. Anthracene was searched via its $S_0 \rightarrow S_1$ transition, which is centered around 308 to 310 nm, but over the wavelength range of 300 to 312 nm, no signal was detected. However, anthracene may be produced in small quantities as its REMPI cross section is about two orders of magnitude less than the overall cross section for the $S_0 \rightarrow S_1$ transition in the REMPI scheme of phenanthrene (*65*).

SUPPLEMENTARY MATERIALS

Supplementary material for this article is available at http://advances.sciencemag.org/cgi/content/full/5/10/eaaw5841/DC1

Supplementary Text

Table S1. Infrared absorption features recorded before and after the irradiation of acetylene (C2H2) and D2-acetylene (C2D2) ices at 5 K.

Table S2. Ion signal detected during [1+1] REMPI at λ = 258.994 nm.

Table S3. Data applied to calculate the irradiation dose per molecule in C_2H_2 and C_2D_2 ices.

Table S4. Yields of specific isomers detected via REMPI.

Fig. S1. Deuterated acetylene ice spectra before (black) and after (red) processing with energetic electrons.

Fig. S2. Temporal profile of the FTIR band at 3030 cm^{-1} during irradiation and TPD.

Fig. S3. Temperature-dependent SPI-ReTOF-MS (PI = 10.49 eV) data of the subliming molecules from unirradiated acetylene ice.

Fig. S4. REMPI-ReTOF-MS spectra versus temperature for carbon monoxide subliming from the substrate used as a calibration compound to confirm the REMPI capabilities of the system.

Fig. S5. Dominant ion signals detected during [1+1] REMPI at λ = 258.994 nm.

Fig. S6. Weak ion signals detected during [1+1] REMPI at λ = 258.994 nm.

References (*66*–*97*)

REFERENCES AND NOTES

1. M. Fulchignoni, F. Ferri, F. Angrilli, A. J. Ball, A. Bar-Nun, M. A. Barucci, C. Bettanini, G. Bianchini, W. Borucki, G. Colombatti, M. Coradini, A. Coustenis, S. Debei, P. Falkner, G. Fanti, E. Flamini, V. Gaborit, R. Grard, M. Hamelin, A. M. Harri, B. Hathi, I. Jernej, M. R. Leese, A. Lehto, P. F. Lion Stoppato, J. J. López-Moreno, T. Mäkinen, J. A. M. McDonnell, C. P. McKay, G. Molina-Cuberos, F. M. Neubauer, V. Pirronello, R. Rodrigo, B. Saggin, K. Schwingenschuh, A. Seiff, F. Simões, H. Svedhem, T. Tokano, M. C. Towner, R. Trautner, P. Withers, J. C. Zarnecki, In situ measurements of the physical characteristics of Titan's environment. *Nature* **438**, 785–791 (2005).
2. J. I. Lunine, R. D. Lorenz, Rivers, lakes, dunes, and rain: Crustal processes in Titan's methane cycle. *Annu. Rev. Earth Planet. Sci.* **37**, 299–320 (2009).
3. R. M. C. Lopes, R. L. Kirk, K. L. Mitchell, A. LeGall, J. W. Barnes, A. Hayes, J. Kargel, L. Wye, J. Radebaugh, E. R. Stofan, M. A. Janssen, C. D. Neish, S. D. Wall, C. A. Wood, J. I. Lunine, M. J. Malaska, Cryovolcanism on Titan: New results from Cassini RADAR and VIMS. *J. Geophys. Res. Planets* **118**, 416–435 (2013).
4. S. M. Hörst, Titan's atmosphere and climate. *J. Geophys. Res. Planets* **122**, 432–482 (2017).
5. A. G. Hayes, R. D. Lorenz, J. I. Lunine, A post-cassini view of Titan's methane-based hydrologic cycle. *Nat. Geosci.* **11**, 306–313 (2018).
6. R. D. Lorenz, S. Wall, J. Radebaugh, G. Boubin, E. Reffet, M. Janssen, E. Stofan, R. Lopes, R. Kirk, C. Elachi, J. Lunine, K. Mitchell, F. Paganelli, L. Soderblom, C. Wood, L. Wye,

H. Zebker, Y. Anderson, S. Ostro, M. Allison, R. Boehmer, P. Callahan, P. Encrenaz, G. G. Ori, G. Francescetti, Y. Gim, G. Hamilton, S. Hensley, W. Johnson, K. Kelleher, D. Muhleman, G. Picardi, F. Posa, L. Roth, R. Seu, S. Shaffer, B. Stiles, S. Vetrella, E. Flamini, R. West, The sand seas of Titan: Cassini RADAR observations of longitudinal dunes. *Science* **312**, 724–727 (2006).

7. S. Rodriguez, A. Garcia, A. Lucas, T. Appéré, A. Le Gall, E. Reffet, L. Le Corre, S. Le Mouélic, T. Cornet, S. Courrech du Pont, C. Narteau, O. Bourgeois, J. Radebaugh, K. Arnold, J. W. Barnes, K. Stephan, R. Jaumann, C. Sotin, R. H. Brown, R. D. Lorenz, E. P. Turtle, Global mapping and characterization of Titan's dune fields with Cassini: Correlation between RADAR and VIMS observations. *Icarus* **230**, 168–179 (2014).
8. R. D. Lorenz, K. L. Mitchell, R. L. Kirk, A. G. Hayes, O. Aharonson, H. A. Zebker, P. Paillou, J. Radebaugh, J. I. Lunine, M. A. Janssen, S. D. Wall, R. M. Lopes, B. Stiles, S. Ostro, G. Mitri, E. R. Stofan, Titan's inventory of organic surface materials. *Geophys. Res. Lett.* **35**, 10.1029/2007GL032118, (2008).
9. V. Vuitton, R. V. Yelle, J. Cui, Formation and distribution of benzene on Titan. *J. Geophys. Res. Planets* **113**, E05007 (2008).
10. V. Vuitton, R. V. Yelle, S. J. Klippenstein, S. M. Hörst, P. Lavvas, Simulating the density of organic species in the atmosphere of Titan with a coupled ion-neutral photochemical model. *Icarus* **324**, 120–197 (2019).
11. A. Le Gall, M. A. Janssen, L. C. Wye, A. G. Hayes, J. Radebaugh, C. Savage, H. Zebker, R. D. Lorenz, J. I. Lunine, R. L. Kirk, R. M. C. Lopes, S. Wall, P. Callahan, E. R. Stofan, T. Farr; Cassini Radar Team, Cassini SAR, radiometry, scatterometry and altimetry observations of Titan's dune fields. *Icarus* **213**, 608–624 (2011).
12. M. G. Tomasko, L. R. Doose, L. E. Dafoe, C. See, Limits on the size of aerosols from measurements of linear polarization in Titan's atmosphere. *Icarus* **204**, 271–283 (2009).
13. L. A. Soderblom, R. L. Kirk, J. I. Lunine, J. A. Anderson, K. H. Baines, J. W. Barnes, J. M. Barrett, R. H. Brown, B. J. Buratti, R. N. Clark, D. P. Cruikshank, C. Elachi, M. A. Janssen, R. Jaumann, E. Karkoschka, S. L. Mouélic, R. M. Lopes, R. D. Lorenz, T. B. McCord, P. D. Nicholson, J. Radebaugh, B. Rizk, C. Sotin, E. R. Stofan, T. L. Sucharski, M. G. Tomasko, S. D. Wall, Correlations between Cassini VIMS spectra and RADAR SAR images: Implications for Titan's surface composition and the character of the Huygens probe landing site. *Planet. Space Sci.* **55**, 2025–2036 (2007).
14. S. Singh, T. B. McCord, J.-P. Combe, S. Rodriguez, T. Cornet, S. L. Mouélic, R. N. Clark, L. Maltagliati, V. F. Chevrier, Acetylene on Titan's surface. *Astrophys. J.* **828**, 55–63 (2016).
15. J. I. Lunine, S. M. Hörst, Organic chemistry on the surface of Titan. *Rendiconti Lincei* **22**, 183–189 (2011).
16. M. E. Brown, E. L. Schaller, G. A. Blake, Irradiation products on dwarf planet Makemake. *Astron. J.* **149**, 105–111 (2015).
17. L. Zhou, W. Zheng, R. I. Kaiser, A. Landera, A. M. Mebel, M.-C. Liang, Y. L. Yung, Cosmic-ray-mediated formation of benzene on the surface of Saturn's moon Titan. *Astrophys. J.* **718**, 1243–1251 (2010).
18. L. Allamandola, A. Tielens, J. Barker, Interstellar polycyclic aromatic hydrocarbons; The infrared emission bands, the excitation/emission mechanism, and the astrophysical implications. *Astrophys. J. Sup.* **71**, 733–775 (1989).
19. R. I. Kaiser, K. Roessler, Theoretical and laboratory studies on the interaction of cosmic-ray particles with interstellar ices. I. Synthesis of polycyclic aromatic hydrocarbons by a cosmic-ray-induced multicenter mechanism. *Astrophys. J.* **475**, 144–154 (1997).
20. C. W. Bauschlicher Jr., S. R. Langhoff, S. A. Sandford, D. M. Hudgins, Infrared spectra of perdeuterated naphthalene, phenanthrene, chrysene, and pyrene. *J. Phys. Chem. A* **101**, 2414–2422 (1997).
21. E. Cané, A. Miani, P. Palmieri, R. Tarroni, A. Trombetti, The gas-phase infrared spectra of phenanthrene-H_{10} and phenanthrene-D_{10}. *Spectrochim. Acta A* **53**, 1839–1851 (1997).
22. E. Cané, A. Miani, A. Trombetti, Anharmonic force fields of naphthalene-H_8 and naphthalene-D_8. *J. Phys. Chem. A* **111**, 8218–8222 (2007).
23. D. M. Hudgins, S. A. Sandford, L. J. Allamandola, Infrared spectroscopy of polycyclic aromatic hydrocarbon cations. 1. Matrix-isolated naphthalene and perdeuterated naphthalene. *J. Phys. Chem.* **98**, 4243–4253 (1994).
24. S. G. Lias, J. E. Bartmess, J. F. Liebman, J. L. Holmes, R. D. Levin, W. G. Mallard, S. A. Kafafi, in *NIST Chemistry WebBook, NIST Standard Reference Database Number 69*, P. J. Linstrom, W. G. Mallard, Eds. (National Institute of Standards and Technology, retrieved 24 November 2018).
25. R. L. Hudson, R. F. Ferrante, M. H. Moore, Infrared spectra and optical constants of astronomical ices: I. Amorphous and crystalline acetylene. *Icarus* **228**, 276–287 (2014).
26. A. Dawes, N. Pascual, S. V. Hoffmann, N. C. Jones, N. J. Mason, Vacuum ultraviolet photoabsorption spectroscopy of crystalline and amorphous benzene. *Phys. Chem. Chem. Phys.* **19**, 27544–27555 (2017).
27. X. Zhang, S. P. Sander, Infrared absorption spectrum of phenanthrene in an argon matrix. *Chem. Phys. Lett.* **688**, 47–50 (2017).
28. M. J. Abplanalp, A. Borsuk, B. M. Jones, R. I. Kaiser, On the formation and isomer specific detection of propenal (C_2H_3CHO) and cyclopropanone (c-C_3H_4O) in interstellar model ices—a combined FTIR and reflectron time-of-flight mass spectroscopic study. *Astrophys. J.* **814**, 45–61 (2015).
29. O. F. Swenson, G. D. Gillispie, Rempi detection of volatile aromatic hydrocarbons in ambient air. *Proc. SPIE* **2835**, 144–153 (1996).
30. T. C. Dinadayalane, U. D. Priyakumar, G. N. Sastry, Exploration of C_6H_6 potential energy surface: A computational effort to unravel the relative stabilities and synthetic feasibility of new benzene Isomers†. *J. Phys. Chem. A* **108**, 11433–11448 (2004).
31. W. B. Tzeng, K. Narayanan, J. L. Lin, Detection of styrene impurities in phenylacetylene by resonance-enhanced multiphoton ionization time-of-flight mass spectrometry. *Applied Spectroscopy* **53**, 731–734 (1999).
32. J. W. Hager, S. C. Wallace, Two-laser photoionization supersonic jet mass spectrometry of aromatic molecules. *Anal. Chem.* **60**, 5–10 (1988).
33. C. M. Klimcak, J. E. Wessel, Gas chromatography with detection by laser excited resonance enhanced 2-photon photoionization. *Anal. Chem.* **52**, 1233–1239 (1980).
34. L. Zhou, R. I. Kaiser, L. G. Gao, A. H. H. Chang, M.-C. Liang, Y. L. Yung, Pathways to oxygen-bearing molecules in the interstellar medium and in planetary atmospheres: Cyclopropenone (c-C_3H_2O) and propynal (HCCCHO). *Astrophys. J.* **686**, 1493–1502 (2008).
35. Y. T. Lee, J. D. McDonald, P. R. LeBreton, D. R. Herschbach, Molecular beam reactive scattering apparatus with electron bombardment detector. *Rev. Sci. Instrum.* **40**, 1402–1408 (1969).
36. C. Sagan, W. Reid Thompson, Production and condensation of organic gases in the atmosphere of Titan. *Icarus* **59**, 133–161 (1984).
37. G. J. Molina-Cuberos, J. J. López-Moreno, R. Rodrigo, L. M. Lara, K. O'Brien, Ionization by cosmic rays of the atmosphere of Titan. *Planet. Space Sci.* **47**, 1347–1354 (1999).
38. J. Oro, in *Bioastronomy 99* (2000), vol. 213.
39. H. B. Niemann, S. K. Atreya, S. J. Bauer, G. R. Carignan, J. E. Demick, R. L. Frost, D. Gautier, J. A. Haberman, D. N. Harpold, D. M. Hunten, G. Israel, J. I. Lunine, W. T. Kasprzak, T. C. Owen, M. Paulkovich, F. Raulin, E. Raaen, S. H. Way, The abundances of constituents of Titan's atmosphere from the GCMS instrument on the Huygens probe. *Nature* **438**, 779–784 (2005).
40. M. Frenklach, D. W. Clary, W. C. Gardiner Jr., S. E. Stein, Detailed kinetic modeling of soot formation in shock-tube pyrolysis of acetylene, in *Symposium (International) on Combustion*, (Elsevier, 1985), vol. 20, pp. 887–901.
41. L. Zhao, R. I. Kaiser, B. Xu, U. Ablikim, M. Ahmed, M. M. Evseev, E. K. Bashkirov, V. N. Azyazov, A. M. Mebel, Low-temperature formation of polycyclic aromatic hydrocarbons in Titan's atmosphere. *Nat. Astron.* **2**, 973–979 (2018).
42. R. H. Brown, K. H. Baines, G. Bellucci, B. J. Buratti, F. Capaccioni, P. Cerroni, R. N. Clark, A. Coradini, D. P. Cruikshank, P. Drossart, V. Formisano, R. Jaumann, Y. Langevin, D. L. Matson, T. B. McCord, V. Mennella, R. M. Nelson, P. D. Nicholson, B. Sicardy, C. Sotin, N. Baugh, C. A. Griffith, G. B. Hansen, C. A. Hibbitts, T. W. Momary, M. R. Showalter, Observations in the saturn system during approach and orbital insertion, with Cassini's visual and infrared mapping spectrometer (VIMS). *Astron. Astrophys.* **446**, 707–716 (2006).
43. O. Grasset, J. Castillo-Rogez, T. Guillot, L. N. Fletcher, F. Tosi, Water and volatiles in the outer solar system. *Space Sci. Rev.* **212**, 835–875 (2017).
44. B. J. Buratti, K. Soderlund, J. Bauer, J. A. Mosher, M. D. Hicks, D. P. Simonelli, R. Jaumann, R. N. Clark, R. H. Brown, D. P. Cruikshank, T. Momary, Infrared (0.83–5.1 μm) photometry of Phoebe from the Cassini visual infrared mapping spectrometer. *Icarus* **193**, 309–322 (2008).
45. D. P. Cruikshank, C. M. Dalle Ore, R. N. Clark, Y. J. Pendleton, Aromatic and aliphatic organic materials on iapetus: Analysis of Cassini VIMS data. *Icarus* **233**, 306–315 (2014).
46. T. B. McCord, G. B. Hansen, R. N. Clark, P. D. Martin, C. A. Hibbitts, F. P. Fanale, J. C. Granahan, M. Segura, D. L. Matson, T. V. Johnson, R. W. Carlson, W. D. Smythe, G. E. Danielson, Non-water-ice constituents in the surface material of the icy galilean satellites from the Galileo near-infrared mapping spectrometer investigation. *J. Geophys. Res. Planets* **103**, 8603–8626 (1998).
47. C. M. Dalle Ore, S. Protopapa, J. C. Cook, W. M. Grundy, D. P. Cruikshank, A. J. Verbiscer, K. Ennico, C. B. Olkin, S. A. Stern, H. A. Weaver, L. A. Young; New Horizons Science Team, Ices on Charon: Distribution of H_2O and NH_3 from new horizons LEISA observations. *Icarus* **300**, 21–32 (2018).
48. S. Protopapa, W. M. Grundy, D. C. Reuter, D. P. Hamilton, C. M. Dalle Ore, J. C. Cook, D. P. Cruikshank, B. Schmitt, S. Philippe, E. Quirico, R. P. Binzel, A. M. Earle, K. Ennico, C. J. A. Howett, A. W. Lunsford, C. B. Olkin, A. Parker, K. N. Singer, A. Stern, A. J. Verbiscer, H. A. Weaver, L. A. Young; New Horizons Science Team, Pluto's global surface composition through pixel-by-pixel Hapke modeling of New Horizons RALPH/LEISA data. *Icarus* **287**, 218–228 (2017).
49. J.-P. Combe, S. Singh, K. E. Johnson, T. B. McCord, M. C. De Sanctis, E. Ammannito, F. G. Carrozzo, M. Ciarniello, A. Frigeri, A. Raponi, F. Tosi, F. Zambon, J. E. C. Scully, C. A. Raymond, C. T. Russell, The surface composition of Ceres' Ezinu quadrangle analyzed by the Dawn mission. *Icarus* **318**, 124–146 (2019).
50. S. S. Sheppard, The colors of extreme outer solar system objects. *Astron. J.* **139**, 1394–1405 (2010).
51. C. J. Bennett, C. S. Jamieson, Y. Osumura, R. I. Kaiser, Laboratory studies on the irradiation of methane in interstellar, cometary and solar system ices. *Astrophys. J.* **653**, 792–811 (2006).
52. C. Morea Dalle Ore, M. A. Barucci, J. P. Emery, D. P. Cruikshank, L. V. D. Ore, F. Merlin, A. Alvarez-Candal, C. de Bergh, D. E. Trilling, D. Perna, S. Fornasier, R. M. E. Mastrapa, E. Dotto, Composition of KBO (50000) Quaoar. *Astron. Astrophys.* **501**, 349–357 (2009).

53. P. Lacerda, The dark red spot on KBO Haumea. *Proc. Int. Astron. Union* **5**, 192–196 (2009).
54. R. I. Kaiser, S. Maity, B. M. Jones, Infrared and reflectron time-of-flight mass spectroscopic analysis of methane (CH_4)–carbon monoxide (CO) ices exposed to ionization radiation – toward the formation of carbonyl-bearing molecules in extraterrestrial ices. *Phys. Chem. Chem. Phys.* **16**, 3399–3424 (2014).
55. P. Groner, I. Stolkin, H. H. Gunthard, Measurement of deposition rate in matrix spectroscopy with a small laser. *J. Phys. E Sci. Instrum.* **6**, 122–123 (1973).
56. S. Maity, R. I. Kaiser, B. M. Jones, Formation of ketene (H_2CCO) in interstellar analogous methane (CH_4)-carbon monoxide (CO) ices: A combined FTIR and reflectron time-of-flight mass spectroscopic study. *Astrophys. J.* **789**, 36–49 (2014).
57. B. M. Jones, R. I. Kaiser, G. Strazzulla, Uv-vis, infrared, and mass spectroscopy of electron irradiated frozen oxygen and carbon dioxide mixtures with water. *Astrophys. J.* **781**, 85–96 (2014).
58. R. I. Kaiser, Experimental investigation on the formation of carbon-bearing molecules in the interstellar medium via neutral – neutral reactions. *Chem. Rev.* **102**, 1309–1358 (2002).
59. D. Drouin, A. R. Couture, D. Joly, X. Tastet, V. Aimez, R. Gauvin, Casino v2.42—a fast and easy-to-use modeling tool for scanning electron microscopy and microanalysis users. *Scanning* **29**, 92–101 (2007).
60. G. J. H. van Nes, PhD thesis, University of Groningen (1978).
61. R. K. McMullan, Å. Kvick, P. Popelier, Structures of cubic and orthorhombic phases of acetylene by single-crystal neutron diffraction. *Acta Crystallogr. B* **48**, 726–731 (1992).
62. H. Katayanagi, Y. Matsumoto, C. A. de Lange, M. Tsubouchi, T. Suzuki, One- and two-color photoelectron imaging of the co molecule via the $B\,^1\Sigma^+$ state. *J. Chem. Phys.* **119**, 3737–3744 (2003).
63. A. de la Cruz, M. Ortiz, J. A. Cabrera, J. Campos, Isotopically-selective two-photon ionization of ^{12}C- and ^{13}C-benzene and hexadeuterobenzene in a time-of-flight mass spectrometer. *Int. J. Mass Spectrom.* **133**, 39–45 (1994).
64. M. C. R. Cockett, H. Ozeki, K. Okuyama, K. Kimura, Vibronic coupling in the ground cationic state of naphthalene: A laser threshold photoelectron [zero kinetic energy (ZEKE)-photoelectron] spectroscopic study. *J. Chem. Phys.* **98**, 7763–7772 (1993).
65. T. W. Adam, M. Clairotte, T. Streibel, M. Elsasser, A. Pommeres, U. Manfredi, M. Carriero, G. Martini, M. Sklorz, A. Krasenbrink, C. Astorga, R. Zimmermann, Real-time analysis of aromatics in combustion engine exhaust by resonance-enhanced multiphoton ionisation time-of-flight mass spectrometry (REMPI-TOF-MS): A robust tool for chassis dynamometer testing. *Anal. Bioanal. Chem.* **404**, 273–276 (2012).
66. M. J. Abplanalp, S. Gozem, A. I. Krylov, C. N. Shingledecker, E. Herbst, R. I. Kaiser, A study of interstellar aldehydes and enols as tracers of a cosmic ray-driven nonequilibrium synthesis of complex organic molecules. *Proc. Natl. Acad. Sci. U. S. A.* **113**, 7727–7732 (2016).
67. C. L. Yaws, *Thermophysical properties of chemicals and hydrocarbons (2)* (Gulf Professional Publishing, Binghamton, US, 2014).
68. A. M. Turner, M. J. Abplanalp, S. Y. Chen, Y. T. Chen, A. H. H. Chang, R. I. Kaiser, A photoionization mass spectroscopic study on the formation of phosphanes in low temperature phosphine ices. *Phys. Chem. Chem. Phys.* **17**, 27281–27291 (2015).
69. M. J. Abplanalp, S. Góbi, R. I. Kaiser, On the formation and the isomer specific detection of methylacetylene (CH_3CCH), propene (CH_3CHCH_2), cyclopropane (c-C_3H_6), vinylacetylene (CH_2CHCCH), and 1,3-butadiene ($CH_2CHCHCH_2$) from interstellar methane ice analogues. *Phys. Chem. Chem. Phys.* **21**, 5378–5393 (2018).
70. E. Rennie, C. Johnson, J. Parker, D. Holland, D. Shaw, M. Hayes, A photoabsorption, photodissociation and photoelectron spectroscopy study of C_6H_6 and C_6D_6. *Chem. Phys.* **229**, 107–123 (1998).
71. J. C. Person, Isotope effect in the photoionization efficiency for benzene. *J. Chem. Phys.* **43**, 2553–2555 (1965).
72. M. Yoshino, J. Takeuchi, H. Suzuki, Absorption cross sections and photoionization efficiencies of benzene and styrene vapor in the vacuum ultraviolet. *J. Phys. Soc.* **34**, 1039–1044 (1973).
73. N. Kanno, K. Tonokura, Vacuum ultraviolet photoionization mass spectra and crosssections for volatile organic compounds at 10.5 eV. *Appl. Spectrosc.* **61**, 896–902 (2007).
74. T. A. Cool, J. Wang, K. Nakajima, C. A. Taatjes, A. McIlroy, Photoionization cross sections for reaction intermediates in hydrocarbon combustion. *Int. J. Mass Spectrom.* **247**, 18–27 (2005).
75. R. Zimmermann, H. J. Heger, A. Kettrup, U. Boesl, A mobile resonance-enhanced multiphoton ionization time-of-flight mass spectrometry device for on-line analysis of aromatic pollutants in waste incinerator flue gases: First results. *Rap. Comm. Mass Spectrom.* **11**, 1095–1102 (1997).
76. L. Cao, F. Mühlberger, T. Adam, T. Streibel, H. Z. Wang, A. Kettrup, R. Zimmermann, Resonance-enhanced multiphoton ionization and vuv-single photon ionization as soft and selective laser ionization methods for on-line time-of-flight mass spectrometry: Investigation of the pyrolysis of typical organic contaminants in the steel recycling process. *Anal. Chem.* **75**, 5639–5645 (2003).
77. O. P. Haefliger, R. Zenobi, Laser mass spectrometric analysis of polycyclic aromatic hydrocarbons with wide wavelength range laser multiphoton ionization spectroscopy. *Anal. Chem.* **70**, 2660–2665 (1998).
78. L. Zhou, R. I. Kaiser, A. T. Tokunaga, Infrared spectroscopy of crystalline and amorphous diacetylene (C_4H_2) and implications for Titan's atmospheric composition. *Planet. Space Sci.* **57**, 830–835 (2009).
79. R. I. Kaiser, K. Roessler, Theoretical and laboratory studies on the interaction of cosmic-ray particles with interstellar ices. III. Suprathermal chemistry-induced formation of hydrocarbon molecules in solid methane (CH_4), ethylene (C_2H_4), and acetylene (C_2H_2). *Astrophys. J.* **503**, 959–975 (1998).
80. S. H. Cuylle, D. Zhao, G. Strazzulla, H. Linnartz, Vacuum ultraviolet photochemistry of solid acetylene: A multispectral approach. *Astron. Astrophys.* **570**, 1–11 (2014).
81. M. J. Abplanalp, R. I. Kaiser, Implications for extraterrestrial hydrocarbon chemistry: Analysis of ethylene (C_2H_4) and D4-ethylene (C_2D_4) ices exposed to ionizing radiation via combined infrared spectroscopy and reflectron time-of-flight mass spectrometry. *Astrophys. J.* **836**, 195–226 (2017).
82. B. M. McMurtry, S. E. J. Saito, A. M. Turner, H. K. Chakravarty, R. I. Kaiser, On the formation of benzoic acid and HIGHER-ORDER benzene carboxylic acids in interstellar model ICE grains. *Astrophys. J.* **831**, 174–183 (2016).
83. S. A. Sandford, M. P. Bernstein, L. J. Allamandola, The mid-infrared laboratory spectra of naphthalene ($C_{10}H_8$) in solid H_2O. *Astrophys. J.* **607**, 346–360 (2004).
84. R. Ruiterkamp, Z. Peeters, M. H. Moore, R. L. H, A quantitative study of proton irradiation and UV photolysis of benzene in interstellar environments. *Astron. Astrophys.* **440**, 391–402 (2005).
85. M. J. Abplanalp, B. M. Jones, R. I. Kaiser, Untangling the methane chemistry in interstellar and solar system ices toward ionizing radiation: A combined infrared and reflectron time-of-flight analysis. *Phys. Chem. Chem. Phys.* **20**, 5435–5468 (2018).
86. G. L. Bottger, D. F. Eggers Jr., Infrared spectra of crystalline C_2H_2, C_2HD, and C_2D_2. *J. Chem. Phys.* **40**, 2010–2017 (1964).
87. K. D. Doney, D. Zhao, J. F. Stanton, H. Linnartz, Theoretical investigation of the infrared spectrum of small polyynes. *Phys. Chem. Chem. Phys.* **20**, 5501–5508 (2018).
88. W. W. Duley, H. Anming, Polyynes and interstellar carbon nanoparticles. *Astrophys. J.* **698**, 808–811 (2009).
89. Y. S. Kim, R. I. Kaiser, An infrared spectroscopic study of amorphous and crystalline ices of vinylacetylene and implications for Saturn's satellite Titan. *Astrophys. J. Sup.* **181**, 543–547 (2009).
90. R. I. Kaiser, G. Eich, A. Gabrysch, K. Roessler, Theoretical and laboratory studies on the interaction of cosmic-ray particles with interstellar ices. II. Formation of atomic and molecular hydrogen in frozen organic molecules. *Astrophys. J.* **484**, 487–498 (1997).
91. D. M. Hudgins, S. A. Sandford, Infrared spectroscopy of matrix isolated polycyclic aromatic hydrocarbons. 1. PAHs containing two to four rings. *J. Phys. Chem. A* **102**, 329–343 (1998).
92. E. Tørneng, C. J. Nielsen, P. Klaeboe, H. Hopf, H. Priebe, The i.r., raman and microwave spectra of 1-butene-3-yne (vinylacetylene) and 1-butene-3-yne-4d. *Spectrochim. Acta A* **36**, 975–987 (1980).
93. Y.-J. Wu, B.-M. Cheng, Infrared absorption spectra of ethynyl radicals isolated in solid Ne: Identification of the fundamental C–H stretching mode. *Chem. Phys. Lett.* **461**, 53–57 (2008).
94. J. L. Hollenberg, D. A. Dows, Absolute infrared intensities in crystalline benzene. *J. Chem. Phys.* **37**, 1300–1307 (1962).
95. M. J. Abplanalp, R. I. Kaiser, Complex hydrocarbon chemistry in interstellar and solar system ices revealed: A combined infrared spectroscopy and reflectron time-of-flight mass spectrometry analysis of ethane (C_2H_6) and D6-ethane (C_2D_6) ices exposed to ionizing radiation. *Astrophys. J.* **827**, 132–161 (2016).
96. Z. Zhou, M. Xie, Z. Wang, F. Qi, Determination of absolute photoionization cross-sections of aromatics and aromatic derivatives. *Rap. Comm. Mass Spectrom.* **23**, 3994–4002 (2009).
97. N. S. R. Laboratory, (2017); http://flame.nsrl.ustc.edu.cn/database/.

Acknowledgments: We acknowledge the W. M. Keck Foundation for financing the experimental setup. **Funding:** We thank the U.S. National Science Foundation (AST-1800975) for support to conduct the experiments and data analysis. **Author contributions:** R.I.K. designed the experiment. R.F. and M.J.A. carried out the experimental measurements. M.J.A. performed the data analyses. M.J.A. and R.I.K. wrote the manuscript. **Competing interests:** The authors declare that they have no competing interests. **Data and materials availability:** All data needed to evaluate the conclusions in the paper are present in the paper and/or the Supplementary Materials. Additional data related to this paper may be requested from the authors.

Submitted 7 January 2019
Accepted 22 September 2019
Published 16 October 2019
10.1126/sciadv.aaw5841

Citation: M. J. Abplanalp, R. Frigge, R. I. Kaiser, Low-temperature synthesis of polycyclic aromatic hydrocarbons in Titan's surface ices and on airless bodies. *Sci. Adv.* **5**, eaaw5841 (2019).